Published in final edited form as:
J Phys Chem C Nanomater Interfaces. 2013 November 7; 117(44): 23279–23285. doi:10.1021/jp406239d.

Particle Lithography Enables Fabrication of Multicomponent Nanostructures

Wei-feng Lin[†], **Logan A. Swartz**[‡], **Jie-Ren Li**[†], **Yang Liu**[†], and **Gang-yu Liu**[†,‡,*]

[†]Department of Chemistry, University of California, Davis, Davis, California 95616, United States

[‡]Biophysics Graduate Group, University of California, Davis, Davis, California 95616, United States

Abstract

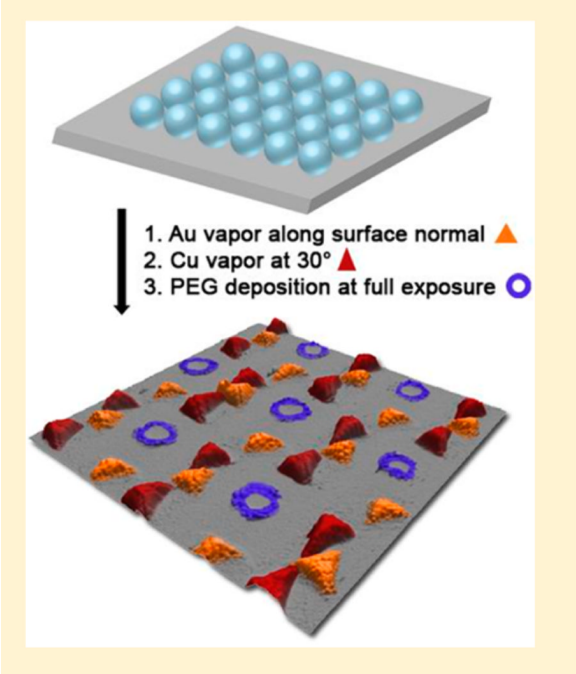

Multicomponent nanostructures with individual geometries have attracted much attention because of their potential to carry out multiple functions synergistically. The current work reports a simple method using particle lithography to fabricate multicomponent nanostructures of metals, proteins, and organosiloxane molecules, each with its own geometry. Particle lithography is well-known for its capability to produce arrays of triangular-shaped nanostructures with novel optical properties. This paper extends the capability of particle lithography by combining a particle template in conjunction with surface chemistry to produce multicomponent nanostructures. The advantages and limitations of this approach will also be addressed.

[*]**Corresponding Author**. gyliu@ucdavis.edu (G.L.).

The authors declare no competing financial interest.

INTRODUCTION

Multicomponent nanostructures arranged in designed geometries and positions have attracted much attention because of their potential in attaining synergistic properties arising from individual components.[1–5] Compared with single- and two-component nanostructures, complex multicomponent nanostructures could enable more functions that are not available in their counterparts.[5] One reason is that different components often have coherent interfaces, resulting in new properties that emerge from intercomponent interactions. An example would be enhanced fluorophore emission induced by the interaction of surface plasmons at metallic nanofilms with vicinal fluorophores located at the metal surface.[6,7] Therefore, multicomponent nanostructures possess multifunctionality through integration of different functional components into a designed complex structure. Multicomponent nanostructures with well-defined geometries will advance a broad range of applications in nanocircuitry[8–11] and biosensing.[12–15]

Techniques utilized in generating multicomponent nanostructures include molecular self-assembly,[16–18] electron-beam (e-beam) lithography,[19,20] and scanning probe lithography such as nanografting[21–24] and dip-pen nanolithography (DPN).[25–28] Molecular self-assembly relies on the interplay between thermodynamics, kinetics, and molecular–molecular as well as molecular–surface interactions in the formation of nanodomains of each component. This method has the advantage of simplicity but is limited to specific molecules that can form self-assembled phases.[17] In addition, the spatial distribution is limited to the structures and segregations formed as a result of the balancing of kinetics and thermodynamics. Thus, it is difficult to control geometry and size.[17] E-beam lithography allows precise geometries and sizes to be produced on the substrate material. However, it is time-consuming, requires expensive instrumentation, and is performed in high vacuum. In addition, patterning biomaterials via e-beam lithography still remains challenging.[4] Scanning probe lithography enables the highest spatial precision and is very versatile in fabricating various components and geometries. However, these methods are relatively low throughput and involve expensive instrumentation. Arrays of probes can remedy the throughput issue to some degree but at the price of compromising density ($\sim 1.1 \times 10^3$ units/mm^2) and spatial resolution.[29–31]

Complementary to the aforementioned methods, particle lithography provides a simple means to produce nanoarrays of metals,[32–37] self-assembled monolayers (SAMs),[38–44] proteins,[45–48] polymers,[49,50] nanoparticles,[51–53] and catalysts[54] for daily lab needs. Since its initial success, particle lithography has been modified, extending its capabilities to binary systems and hierarchical micro/nanostructures. By stepwise angle-resolved particle lithography, binary arrays of Au and Ag nanostructures were fabricated.[33] Recently, we have reported that by sequential deposition of two metal vapors through two different particle templates, binary nanopatterns were produced to allow the observation of the Moiré effect at the nanometer scale.[37] Combining microcontact printing and particle lithography, hierarchical micro- and nanostructures with two different components were produced in one printing step.[55]

This paper represents further extension of particle lithography to produce multicomponent nanostructures of metals, proteins, and organosiloxane molecules with individual geometries. The choice of materials is based upon the fact that metals are key components in nanoelectronic and nano-photonics devices.[56,57] In addition, arrays of multicomponent proteins are key components in protein-based nanobiodevices such as sensors and assay-based analysis tools.[58–61]

Particle lithography was used in sequence, in conjunction with design surface chemistry such as protein immobilization and silane chemistry. The resulting nanostructures were characterized using high-resolution AFM. Five types of nanostructures are discussed to reveal the enabling aspects and advantages of this approach. In comparison with the aforementioned approaches, this method provides advantages of (1) simplicity without any expensive equipment or ultrahigh vacuum, (2) practical throughput for daily research lab uses, (3) versatility of patterning a broad range of materials, and (4) enabling a certain degree of control over feature size and geometry.

EXPERIMENTAL SECTION

Materials

Glass coverslips (No.1) were purchased from Corning (Corning, NY) with lateral dimensions of 18 mm × 18 mm and thicknesses of 0.18 mm. Au slugs (99.999%) and Cu slugs (99.999%) were purchased from Alfa Aesar (Ward Hill, MA). Ethanol (EtOH, 99.99%) was purchased from Gold Shield Chemical Co. (Hayward, CA). Sulfuric acid (95.0%), hydrogen peroxide (30% aqueous solution), ammonium hydroxide (30% aqueous solution), tetrahydrofuran (THF, 99.5%), and toluene (HPLC grade) were purchased from EMD Chemicals (Gibbstown, NJ) and used as received. Bovine serum albumin (BSA) was purchased from Sigma-Aldrich (St. Louis, MO). 2-[Methoxy(polyethyleneoxy)propyl]-trichlorosilane (PEG-silane) was purchased from Gelest (Morrisville, PA) and used as received. Water (≥18.2 MΩ· cm) was generated from a Milli-Q system (Q-GARD 2, Millipore, Billerica, MA) and used for dilution and washing. Nitrogen gas (99.999%) and hydrogen gas (99.95%) were purchased from Praxair, Inc. (Danbury, CT). Silica microspheres with diameters of 0.73 ± 0.02 and 1.57 ± 0.02 μm were purchased from Thermo Scientific (Waltham, MA). The spheres were suspended in their original concentration of 2% (w/v, aqueous) until usage.

Preparation of Multicomponent Patterns

Glass cover-slips were used as substrates and cleaned following previously reported protocols.[45,51,55] In brief, substrates were cleaned by immersion in piranha solution for 1 h and subsequently in basic bath at 70 °C for 1 h. Piranha solution is a mixture of sulfuric acid and hydrogen peroxide at a (v/v) ratio of 3:1. It is highly corrosive and should be handled carefully. The basic bath is a mixture of ammonium hydroxide, hydrogen peroxide, and water at a (v/v/v) ratio of 5:1:1. Substrates were then rinsed with copious quantities of ultrapure water and dried in nitrogen gas.

The multicomponent patterns were fabricated on glass substrates by using particle lithography. Briefly, template spheres were washed by centrifugation to remove charge stabilizer and surfactants using previously reported protocols.[37,38,42] Removal of charge stabilizer and surfactants improves the quality of the packing. After cleaning, template particles were resuspended in aqueous solutions by vortex mixing or sonication and used shortly after to avoid aggregation. A drop of the sphere solution was deposited on a clean substrate immediately and dried in ambient conditions to produce masks for lithography. Sequential deposition of metal vapors and drop casting BSA through the same particle template was performed to prepare multicomponent patterns. Drop casting has been used for soluble components in particle lithography,[45,46,48] and key steps include pipetting BSA solution onto the glass surface and letting dry in an ambient and clean environment. The patterns are composed of Au, Cu, and BSA arrays with periodicity of 1.57 μm while using a monolayer of silica spheres (D = 1.57 μm) as the template for sequential deposition. A 53 nm Cu thin film was deposited onto the template in a high-vacuum evaporator (model DV502-A, Denton Vacuum Inc., Moorestown, NJ) at 10^{-7} Torr and room temperature. The

incidence angle of the deposition was controlled to be 30° with respect to surface normal. The evaporation rate was monitored by a quartz crystal monitor (Inficon Inc., East Syracuse, NY) and controlled between 0.10 and 0.15 nm/s. After the deposition of Cu, a 53 nm Au thin film was deposited onto the sample, with deposition angle 0° from the normal. After Au deposition, 100 μL of 2 mg/mL BSA solution was drop cast onto the sample and allowed to dry overnight. The multicomponent patterns were revealed after the silica spheres mask was removed by sonication in H_2O for 3 s. To retain bioactivity and prevent detachment, sonication time was kept under 1 min.[45]

Sample Characterization with Atomic Force Microscopy (AFM)

Samples were characterized by an atomic force microscope (MFP-3D, Asylum Research Corp., Santa Barbara, CA). All the AFM images were acquired under contact mode with imaging forces of 15–25 nN. Si_3N_4 cantilevers with a spring constant of 0.1 N/m were purchased from Bruker (NP and MSNL, Camarillo, CA). The AFM images were acquired and analyzed using Asylum MFP3D software developed on the Igor Pro 6.12 platform.

RESULTS AND DISCUSSION

Particle Lithography Enables Fabrication of Multicomponent Nanostructures

Key steps for producing multicomponent nanostructures are illustrated in Figure 1 using Au, Cu, and BSA as examples. Au and Cu hybrid nanostructures are known to have a synergistic plasmonic enhancement[62] and good thermal stability.[63] BSA is commonly used as a backfilling agent in protein immobolization reactions in biosensors.[64–66] It is known to maintain bioactivity after deposition onto solid surfaces.[67] More details about the fabrication process can be found in the Experimental Section. First, a monolayer of close-packed silica spheres was formed by dropping 35 μL of silica sphere solution onto a glass surface. These silica spheres served as a mask for subsequent Cu vapor deposition via thermal evaporation.[32,35–37] The incident angle of the deposition can be varied from 0° to 55°.[32] In creating the patterns in Figure 1, we chose 30° with respect to the surface normal. The projected particle interstices determine the size, geometry, and spacing of the Cu islands.[32] After Cu deposition, Au thin films were deposited through the same particle mask, but along a different incidence, e.g., along surface normal. BSA solution is then drop cast through the same particle mask and allowed to dry. The final structure was characterized after mask removal. Note only one template D = 1.57 μm silica microspheres was used throughout the lithographic process.

Figure 2 shows the triple-component nanostructures visualized using AFM. The patterns contain three periodic arrays with the same periodicity 1.57 ± 0.03 μm, which were dictated by the diameter of the silica microspheres. Figure 2A is a 50 × 50 μm^2 AFM image of the patterns, showing a highly ordered structure formed across the region. It demonstrates the high-throughput of the method. Figure 2B is the close-up view of the patterns, where detailed structures of each component are clearly visible. The Au feature is an equilateral triangle (blue). The side lengths of the equilateral triangles equal to 330 ± 34 nm. The thickness measures 53 ± 1 nm. The geometry is consistent with previous reports using similar incidence and protocol.[34,35,37] The Cu islands are isosceles triangular-shaped, as highlighted in orange. The side lengths of the triangles are $a = b$ = 331 ± 23 nm and c = 252 ± 21 nm, with thickness of 53 ± 1 nm. The deviation from equilateral triangle is controlled by adjusting the incident angle during the vapor deposition. By increasing the incident angle, more distortion from equilateral triangles is observed. The BSA molecules cover the entire surface except for the dark circles (highlighted in green). The diameter of the circle is 472 ± 51 nm, and the depth measures 7 ± 1 nm. This corresponds to two layers of BSA molecules since the diameter of BSA is 4 nm according to X-ray crystallography measurements.[68]

Upon deposition, the close-packed particles provide a structural template to guide adsorption of BSA molecules on surface. The proteins adsorb and pack closely onto uncovered interstitial areas surrounding the base of the particle templates. The particles are removed to leave protein nanostructures on the surface. Two layers of BSA molecules remain securely attached to the surface with imprinted pore-shaped structures that conform to the circular shape of the particle templates when the spheres are removed.[45,48] The dark regions correspond to the uncovered area previously occupied by the particles. The density of the nanostructures calculated is 6.6×10^6 feature/mm^2.

Particle lithography is a straightforward tool in patterning multicomponent nanostructures. The size, shape, and spacing of the nanopattern can be controlled at the nanometer scale by the diameter of the particle mask, as demonstrated in Figure 2C,D. For particle templates with diameters as small as 0.73 μm, particle lithography was applied successfully with the overall morphology of hexagonal arrangement of BSA circles overlapped with Au and Cu dot arrays in honeycomb morphology. A 5×5 μm^2 AFM image in Figure 2C displays the uniformity and periodicity of the patterned surface. The average periodicity of the patterns measures 760 ± 28 nm. The density of the nanostructures is calculated to be 3.1×10^7 feature/mm^2. A zoom-in topograph (2.5×2.5 μm^2) in Figure 2D reveals the structural details of the patterns. Each component exhibits the distinct geometric feature in the same region. The morphology of Au islands is equilateral triangles, as highlighted in blue. The side lengths of the equilateral triangles are equal to 162 ± 23 nm with thickness of 52 ± 8 nm. The Cu islands display isosceles triangle-shaped morphology, as highlighted in orange. The side lengths of the isosceles triangles are $a = b = 157 \pm 10$ nm and $c = 130 \pm 9$ nm, with the thickness equal to 52 ± 10 nm. The BSA arrays with a hexagonal arrangement of circles are highlighted in green. The diameter of the circle is 194 ± 23 nm with depth equal to 3.7 ± 0.6 nm. It is apparent that particle lithography is a highly reproducible approach to fabricate multicomponent patterns. The arrangement of each component reflects the long-range order, dimensions, and periodicity according to the hexagonal packing of template spheres.

Particle Lithography Enables Fabrication of Arrays with Different Material Combinations

The capability of particle lithography in patterning a broad range of materials enables fabrication of multicomponent structures with different material combinations. By using different material deposition methods, geometry and the size of the features within the patterns can be manipulated. Figure 3A–D represents four basic single-component patterns generated using the $D = 1.57$ μm silica particles as templates. The patterns of equilateral triangular arrays in Figure 3A were fabricated by vapor deposition of Au through a monolayer particle mask. Hexagonal dot arrays in Figure 3B were fabricated by vapor deposition of Au through a double-layer particle template. The sample in Figure 3C shows circular arrays of octadecyltrichlorosilane (OTS) fabricated via deposition of OTS vapor through a particle mask. Circular arrays of BSA shown in Figure 3D were fabricated by drop casting of BSA solution through the particle template.

By combining the above-described steps, binary arrays with distinct geometric features for each component can be produced, as shown in Figure 3E,G. Figure 3E shows Au and PEG-silane arrays with periodicity of 1.57 μm. The patterns were prepared by thermal deposition of 47 nm of Au thin film through a monolayer particle mask, followed by vapor deposition of PEG-silane molecules through the same mask. After the silica spheres mask was removed by sonication in ethanol, the nanopatterns were revealed. The circular arrays correspond to PEG-silane arrays, with inner ring diameter of 155 ± 14 nm, outer ring diameter of 316 ± 26 nm, and height of the rings measured at 3 ± 1 nm. The equilateral triangular arrays are Au arrays; the side lengths of triangles equal to 340 ± 26 nm and thickness 65 ± 2 nm.

The patterns shown in Figure 3G are composed of OTS and BSA with periodicity of 1.57 μm. The sample was prepared by vapor deposition of OTS molecules, followed by drop casting of 50 μL of 0.2 mg/mL BSA through the same mask. The patterns were imaged after the silica spheres were removed by sonication in water. In these patterns, ring arrays of OTS were surrounded by circular structures of BSA. The inner diameter of the OTS ring measures 133 ± 7 nm, with the line width and height being 77 ± 8 nm, and 1.0 ± 0.2 nm, respectively. In between the OTS and the BSA region, a circular band region, 436 ± 12 nm wide, appears darker in the AFM image. This region is uncovered or low coverage glass surface. The rest of the surface is covered by BSA molecules. Patterns shown in Figure 3F contain Au and OTS arrays with periodicity of 1.57 μm. The sample was prepared by thermal deposition of a 47 nm of Au thin film through a double-layered particle mask, followed by vapor deposition of OTS molecules through the same mask. After the silica particle mask was removed by sonication in ethanol, the patterns were revealed. The circular arrays are OTS arrays, with inner ring diameter of 181 ± 12 nm, outer ring diameter of 606 ± 41 nm, and a height of 6.8 ± 0.8 nm. The hexagonal dot arrays are Au arrays; the dimension of the dots is 75 ± 22 nm, and the thickness of the dots is equal to 57 ± 7 nm.

By selective introduction of the third material through the same particle mask, one can produce designed tri-component patterns. Figure 3H shows triple-component patterns composed of Au, Cu, and PEG-silane arrays with periodicity of 1.57 μm. The sample was prepared by sequential deposition of Cu and Au and PEG-silane vapors through the same particle template. Deposition of Cu and Au through colloidal templates results in formation of triangular-shaped nanostructures. During the PEG-silane vapor deposition, water meniscus formed following the base of the sphere at the sphere–surface contact to initiate local surface hydrolysis of PEG-silane to bind to substrates. The meniscus exhibits circular geometry whose width depends on the humidity and local surface tension and, as such, results in the formation of the ring-shaped siloxane nanostructures.[38,42] The area between the substrate and the base of the spheres is an effective guide to form the nanostructures with circular geometry. After mask removal, the resulting structure is a combination of equilateral triangular arrays of Au, isosceles triangular arrays of Cu, and circular arrays of PEG-silane. As shown in Figure 3H, three materials with three different geometric features are observed in the same region. The Au islands are equilateral triangular-shaped, as highlighted in blue. The side lengths of the equilateral triangles equal 354 ± 49 nm while thickness measures 44 ± 3 nm. The Cu islands are an isosceles triangular shape, as highlighted in orange. The side lengths of the isosceles triangles are $a = b = 419 \pm 21$ nm and $c = 328 \pm 17$ nm, with thickness of 44 ± 4 nm. The PEG-silane arrays are circular structures, as highlighted in red. The outer diameter of the rings is 493 ± 18 nm, and the inner diameter of the rings is 229 ± 40 nm, with depth equal to 13 ± 2 nm. This demonstrates that geometry of individual features within the patterns can be controlled by simply utilizing different material deposition methods.

While particle lithography provides a simple tool for production of multicomponent nanostructures with practical throughput, limitations are present. Since the periodicity is dictated by the diameter of the template particles, it is difficult to produce patterns with various periodicities within one template cycle. The current remedy is to use multiple steps each with designed particle diameter, which makes this protocol longer than desirable. In addition, the geometry of the features and distribution of defects have profound dependences on the packing and registry of the particle template. For example, triangular structures correlate to the projection of the particle mask interstices onto the substrate, while circular structures correspond to the contact region between the particles and substrate. It is still challenging to produce designed geometries. Effort is ongoing to adjust the surface reactions under the templates to expand the horizons of the geometries.

CONCLUSIONS

A simple method using particle lithography sequentially in conjunction with surface chemistry was developed to fabricate multicomponent nanostructures. A film of monodispersed particles serves as a material guide for the deposition of different materials in a designed sequence. After the particle mask is displaced, multicomponent nanostructures are revealed, each component with well-defined size and geometry. Feature size and geometry of the patterns can be manipulated by adjusting the size of the particle template and deposition methods. Such a method has the advantages of simplicity, high throughput, and a capability of patterning a broad range of materials. Work is in progress to expand the applications of the multicomponent nanostructures.

Acknowledgments

We thank Drs. Guohua Yang and Jian Liang at UC Davis for many helpful discussions. We appreciate Ms. Susan Stagner's careful proofreading of the manuscript. This work was supported by the National Science Foundation (CHE-0809977, DMR-1104260), NIH (R21C1976850), and W. M. Keck Foundation.

REFERENCES

1. Zhou M, Dong SJ. Bioelectrochemical Interface Engineering: Toward the Fabrication of Electrochemical Biosensors, Biofuel Cells, and Self-Powered Logic Biosensors. Acc. Chem. Res. 2011; 44:1232–1243. [PubMed: 21812435]
2. Mondal PC, Lakshmanan JY, Hamoudi H, Zharnikov M, Gupta T. Bottom-Up Assembly of Multicomponent Coordination-Based Oligomers. J. Phys. Chem. C. 2011; 115:16398–16404.
3. Chen MW, Le DQS, Hein S, Li PC, Nygaard JV, Kassem M, Kjems J, Besenbacher F, Bunger C. Fabrication and Characterization of a Rapid Prototyped Tissue Engineering Scaffold with Embedded Multicomponent Matrix for Controlled Drug Release. Int. J. Nanomed. 2012; 7:4285–4297.
4. Kim DH, Lee H, Lee YK, Nam JM, Levchenko A. Biomimetic Nanopatterns as Enabling Tools for Analysis and Control of Live Cells. Adv. Mater. 2010; 22:4551–4566. [PubMed: 20803528]
5. Zeng H, Sun SH. Syntheses, Properties and Potential Applications of Multicomponent Magnetic Nanoparticles. Adv. Funct. Mater. 2008; 18:391–400.
6. Rangelowa-Jankowska S, Jankowski D, Bogdanowicz R, Grobelna B, Bojarski P. Surface Plasmon-Coupled Emission of Rhodamine 110 Aggregates in a Silica Nanolayer. J. Phys. Chem. Lett. 2012; 3:3626–3631.
7. Lakowicz JR, Malicka J, Gryczynski I, Gryczynski Z. Directional Surface Plasmon-Coupled Emission: A New Method for High Sensitivity Detection. Biochem. Biophys. Res. Commun. 2003; 307:435–439. [PubMed: 12893239]
8. Chang YJ, Li WL. Directional-Coupler-Based Polarization Splitting in Asymmetric Metal/Multi-Insulator Configuration for Optical Nanocircuitry. IEEE Photonics Technol. Lett. 2012; 24:458–460.
9. Gjonaj B, Aulbach J, Johnson PM, Mosk AP, Kuipers L, Lagendijk A. Active Spatial Control of Plasmonic Fields. Nat. Photonics. 2011; 5:360–363.
10. Huang JS, Callegari V, Geisler P, Bruning C, Kern J, Prangsma JC, Wu XF, Feichtner T, Ziegler J, Weinmann P, et al. Atomically Flat Single-Crystalline Gold Nanostructures for Plasmonic Nanocircuitry. Nat. Commun. 2010; 1
11. Petitjean A, Puntoriero F, Campagna S, Juris A, Lehn JM. Multicomponent Supramolecular Devices: Synthesis, Optical, and Electronic Properties of Bridged Bis-Dirhodium and -Diruthenium Complexes. Eur. J. Inorg. Chem. 2006:3878–3892.
12. Park SJ, Duncan TV, Sanchez-Gaytan BL. Bifunctional Nanostructures Composed of Fluorescent Core and Metal Shell Subdomains with Controllable Geometry. J. Phys. Chem. C. 2008; 112:11205–11210.

13. Wang L, Guo SJ, Hu XO, Dong SJ. Layer-by-Layer Assembly of Carbon Nanotubes and Prussian Blue Nanoparticles: A Potential Tool for Biosensing Devices. Colloids Surf., A. 2008; 317:394–399.
14. Qian ZR, Tan TC. A Model for Multicomponent Biosensing and Its Application to a Dead Cell-Based BOD Biosensor. Chem. Eng. Sci. 1998; 53:3281–3294.
15. Quinn A, Such GK, Quinn JF, Caruso F. Polyelectrolyte Blend Multilayers: A Versatile Route to Engineering Interfaces and Films. Adv. Funct. Mater. 2008; 18:17–26.
16. Lei SB, Tahara K, Feng XL, Furukawa SH, De Schryver FC, Mullen K, Tobe Y, De Feyter S. Molecular Clusters in Two-Dimensional Surface-Confined Nanoporous Molecular Networks: Structure, Rigidity, and Dynamics. J. Am. Chem. Soc. 2008; 130:7119–7129. [PubMed: 18465857]
17. Ciesielski A, Palma CA, Bonini M, Samori P. Towards Supramolecular Engineering of Functional Nanomaterials: Pre-Programming Multi-Component 2D Self-Assembly at Solid-Liquid Interfaces. Adv. Mater. 2010; 22:3506–3520. [PubMed: 20626011]
18. Adisoejoso J, Tahara K, Okuhata S, Lei S, Tobe Y, De Feyter S. Two-Dimensional Crystal Engineering: A Four-Component Architecture at a Liquid-Solid Interface. Angew. Chem., Int. Ed. 2009; 48:7353–7357.
19. Barbagini F, Bengoechea-Encabo A, Albert S, Lefebvre P, Martinez J, Sanchez-Garcia MA, Trampert A, Calleja E. E-Beam Nano-Patterning for the Ordered Growth of GaN/InGaN Nanorods. Microelectron. Eng. 2012; 98:374–377.
20. Huth M, Porrati F, Schwalb C, Winhold M, Sachser R, Dukic M, Adams J, Fantner G. Focused Electron Beam Induced Deposition: A Perspective. Beilstein J. Nanotechnol. 2012; 3:597–619. [PubMed: 23019557]
21. Scaini D, Castronovo M, Casalis L, Scoles G. Electron Transfer Mediating Properties of Hydrocarbons as a Function of Chain Length: A Differential Scanning Conductive Tip Atomic Force Microscopy Investigation. ACS Nano. 2008; 2:507–515. [PubMed: 19206577]
22. Xu S, Miller S, Laibinis PE, Liu GY. Fabrication of Nanometer Scale Patterns within Self-Assembled Monolayers by Nanografting. Langmuir. 1999; 15:7244–7251.
23. Liu GY, Xu S, Qian YL. Nanofabrication of Self-Assembled Monolayers Using Scanning Probe Lithography. Acc. Chem. Res. 2000; 33:457–466. [PubMed: 10913234]
24. Bano F, Fruk L, Sanavio B, Glettenberg M, Casalls L, Niemeyer CM, Scoles G. Toward Multiprotein Nanoarrays Using Nanografting and DNA Directed Immobilization of Proteins. Nano Lett. 2009; 9:2614–2618. [PubMed: 19583282]
25. Piner RD, Zhu J, Xu F, Hong SH, Mirkin CA. “Dippen” Nanolithography. Science. 1999; 283:661–663. [PubMed: 9924019]
26. Hong SH, Zhu J, Mirkin CA. Multiple Ink Nanolithography: Toward a Multiple-Pen Nano-Plotter. Science. 1999; 286:523–525. [PubMed: 10521346]
27. Hong SH, Mirkin CA. A Nanoplotter with Both Parallel and Serial Writing Capabilities. Science. 2000; 288:1808–1811. [PubMed: 10846159]
28. Giam LR, Mirkin CA. Cantilever-Free Scanning Probe Molecular Printing. Angew. Chem., Int. Ed. 2011; 50:7482–7485.
29. Shim W, Brown KA, Zhou XZ, Rasin B, Liao X, Mirkin CA. Multifunctional Cantilever-Free Scanning Probe Arrays Coated with Multilayer Graphene. Proc. Natl. Acad. Sci. U. S. A. 2012; 109:18312–18317. [PubMed: 23086161]
30. Giam LR, Massich MD, Hao LL, Wong LS, Mader CC, Mirkin CA. Scanning Probe-Enabled Nanocombinatorics Define the Relationship Between Fibronectin Feature Size and Stem Cell Fate. Proc. Natl. Acad. Sci. U. S. A. 2012; 109:4377–4382. [PubMed: 22392973]
31. Shim W, Braunschweig AB, Liao X, Chai JN, Lim JK, Zheng GF, Mirkin CA. Hard-Tip, Soft-Spring Lithography. Nature. 2011; 469:516–521. [PubMed: 21270890]
32. Haynes CL, McFarland AD, Smith MT, Hulteen JC, Van Duyne RP. Angle-Resolved Nanosphere Lithography: Manipulation of Nanoparticle Size, Shape, and Interparticle Spacing. J. Phys. Chem. B. 2002; 106:1898–1902.
33. Zhang G, Wang DY. Fabrication of Heterogeneous Binary Arrays of Nanoparticles via Colloidal Lithography. J. Am. Chem. Soc. 2008; 130:5616–5617. [PubMed: 18384201]

34. Hulteen JC, Vanduyne RP. Nanosphere Lithography - A Materials General Fabrication Process for Periodic Array Surfaces. J. Vac. Sci. Technol., A. 1995; 13:1553–1558.
35. Haynes CL, Van Duyne RP. Nanosphere Lithography: A Versatile Nanofabrication Tool for Studies of Size-Dependent Nanoparticle Optics. J. Phys. Chem. B. 2001; 105:5599–5611.
36. Hulteen JC, Treichel DA, Smith MT, Duval ML, Jensen TR, Van Duyne RP. Nanosphere Lithography: Size-Tunable Silver Nanoparticle and Surface Cluster Arrays. J. Phys. Chem. B. 1999; 103:3854–3863.
37. Lin WF, Li JR, Liu GY. Near-Field Scanning Optical Microscopy Enables Direct Observation of Moiré Effects at the Nanometer Scale. ACS Nano. 2012; 6:9141–9149. [PubMed: 22973942]
38. Li JR, Garno JC. Elucidating the Role of Surface Hydrolysis in Preparing Organosilane Nanostructures via Particle Lithography. Nano Lett. 2008; 8:1916–1922. [PubMed: 18563943]
39. Bae C, Shin HJ, Moon J, Sung MM. Contact Area Lithography (CAL): A New Approach to Direct Formation of Nanometric Chemical Patterns. Chem. Mater. 2006; 18:1085–1088.
40. McLellan JM, Geissler M, Xia YN. Edge Spreading Lithography and Its Application to the Fabrication of Mesoscopic Gold and Silver Rings. J. Am. Chem. Soc. 2004; 126:10830–10831. [PubMed: 15339153]
41. Geissler M, McLellan JM, Chen JY, Xia YN. Side-By-Side Patterning of Multiple Alkanethiolate Monolayers on Gold by Edge-Spreading Lithography. Angew. Chem. Int. Ed. 2005; 44:3596–3600.
42. Li JR, Lusker KL, Yu JJ, Garno JC. Engineering the Spatial Selectivity of Surfaces at the Nanoscale Using Particle Lithography Combined with Vapor Deposition of Organosilanes. ACS Nano. 2009; 3:2023–2035. [PubMed: 19572752]
43. Lusker KL, Li JR, Garno JC. Nanostructures of Functionalized Gold Nanoparticles Prepared by Particle Lithography with Organosilanes. Langmuir. 2011; 27:13269–13275. [PubMed: 21928785]
44. Li JR, Garno JC. Nanostructures of Octadecyltrisiloxane Self-Assembled Monolayers Produced on Au(111) Using Particle Lithography. ACS Appl. Mater. Interfaces. 2009; 1:969–976. [PubMed: 20356025]
45. Li JR, Henry GC, Garno JC. Fabrication of Nanopatterned Films of Bovine Serum Albumin and Staphylococcal Protein A using Latex Particle Lithography. Analyst. 2006; 131:244–250. [PubMed: 16440089]
46. Garno JC, Amro NA, Wadu-Mesthrige K, Liu GY. Production of Periodic Arrays of Protein Nanostructures using Particle Lithography. Langmuir. 2002; 18:8186–8192.
47. Taylor ZR, Keay JC, Sanchez ES, Johnson MB, Schmidtke DW. Independently Controlling Protein Dot Size and Spacing in Particle Lithography. Langmuir. 2012; 28:9656–9663. [PubMed: 22656270]
48. Ngunjiri JN, Daniels SL, Li JR, Serem WK, Garno JC. Controlling the Surface Coverage and Arrangement of Proteins using Particle Lithography. Nanomedicine. 2008; 3:529–541. [PubMed: 18694315]
49. Sun ZQ, Li Y, Zhang JH, Li YF, Zhao ZH, Zhang K, Zhang G, Guo JR, Yang B. A Universal Approach to Fabricate Various Nanoring Arrays Based on a Colloidal-Crystal-Assisted-Lithography Strategy. Adv. Funct. Mater. 2008; 18:4036–4042.
50. Mornet S, Bretagnol F, Mannelli I, Valsesia A, Sirghi L, Colpo P, Rossi F. Large-Scale Fabrication of Bi-Functional Nanostructured Polymer Surfaces for Selective Biomolecular Adhesion. Small. 2008; 4:1919–1924. [PubMed: 18980234]
51. Mullen TJ, Zhang M, Feng W, El-khouri RJ, Sun LD, Yan CH, Patten TE, Liu GY. Fabrication and Characterization of Rare-Earth-Doped Nanostructures on Surfaces. ACS Nano. 2011; 5:6539–6545. [PubMed: 21780743]
52. Lewandowski BR, Kelley AT, Singleton R, Li J-R, Lowry M, Warner IM, Garno JC. Nanostructures of Cysteine-Coated CdS Nanoparticles Produced with “Two-Particle” Lithography. J. Phys. Chem. C. 2009; 113:5933–5940.
53. Chan Y-H, Chen J, Wark SE, Skiles SL, Son DH, Batteas JD. Using Patterned Arrays of Metal Nanoparticles to Probe Plasmon Enhanced Luminescence of CdSe Quantum Dots. ACS Nano. 2009; 3:1735–1744. [PubMed: 19499906]

54. Gustavsson M, Fredriksson H, Kasemo B, Jusys Z, Kaiser J, Jun C, Behm RJ. Nanostructured Platinum-on-Carbon Model Electrocatalysts Prepared by Colloidal Lithography. J. Electroanal. Chem. 2004; 568:371–377.
55. Li J-R, Yin N-N, Liu G-Y. Hierarchical Micro- and Nanoscale Structures on Surfaces Produced Using a One-Step Pattern Transfer Process. J. Phys. Chem. Lett. 2011; 2:289–294.
56. Mistark PA, Park S, Yalcin SE, Lee DH, Yavuzcetin O, Tuominen MT, Russell TP, Achermann M. Block-Copolymer-Based Plasmonic Nanostructures. ACS Nano. 2009; 3:3987–3992. [PubMed: 19947582]
57. Qu L, Vaia RA, Dai L. Multilevel, Multicomponent Microarchitectures of Vertically-Aligned Carbon Nanotubes for Diverse Applications. ACS Nano. 2011; 5:994–1002. [PubMed: 21280670]
58. Avseenko NV, Morozova TY, Ataullakhanov FI, Morozov VN. Immunoassay with Multicomponent Protein Micro-arrays Fabricated by Electrospray Deposition. Anal. Chem. 2002; 74:927–933. [PubMed: 11924994]
59. Baldacchini C, Herrero Chamorro MA, Prato M, Cannistraro S. Highly Conductive Redox Protein–Carbon Nanotube Complex for Biosensing Applications. Adv. Funct. Mater. 2011; 21:153–157.
60. Paternolli C, Ghisellini P, Nicolini C. Nanostructuring of Heme-Proteins for Biodevice Applications. Nanobiotechnology. 2007; 1:22–26. [PubMed: 17428121]
61. Rinaldi R, Pompa PP, Maruccio G, Biasco A, Visconti P, Pisignano D, Blasi L, Sgarbi N, Krebs B, Cingolani R. Self-Assembling of Proteins and Enzymes at Nanoscale for Biodevice Applications. IEE Proc.: Nanobiotechnol. 2004; 151:101–108. [PubMed: 16475851]
62. Nawrocka MS, Shrestha S, Panepucci RR, Widera J. Plasmon-Based Light Enhancement from a Hybrid Copper-Gold Planar Structure. Proc. SPIE. 2011; 8096:809634.
63. Kolb DM, Ullmann R, Will T. Nanofabrication of Small Copper Clusters on Gold(111) Electrodes by a Scanning Tunneling Microscope. Science. 1997; 275:1097–1099. [PubMed: 9027304]
64. Hollmann O, Gutberlet T, Czeslik C. Structure and Protein Binding Capacity of a Planar PAA Brush. Langmuir. 2006; 23:1347–1353. [PubMed: 17241057]
65. Mansur HS, Lobato ZP, Oréfice RL, Vasconcelos WL, Oliveira C, Machado LJ. Surface Functionalization of Porous Glass Networks: Effects on Bovine Serum Albumin and Porcine Insulin Immobilization. Biomacromolecules. 2000; 1:789–797. [PubMed: 11710213]
66. Voute N, Bataille D, Girot P, Boschetti E. Characterization of Very Dense Mineral Oxide–Gel Composites for Fluidized-Bed Adsorption of Biomolecules. Bioseparation. 1999; 8:121–129. [PubMed: 10734563]
67. Kang F, Singh J. Conformational Stability of a Model Protein (Bovine Serum Albumin) during Primary Emulsification Process of PLGA Microspheres Synthesis. Int. J. Pharm. 2003; 260:149–156. [PubMed: 12818819]
68. Carter D, He X, Munson S, Twigg P, Gernert K, Broom M, Miller T. Three-Dimensional Structure of Human Serum Albumin. Science. 1989; 244:1195–1198. [PubMed: 2727704]

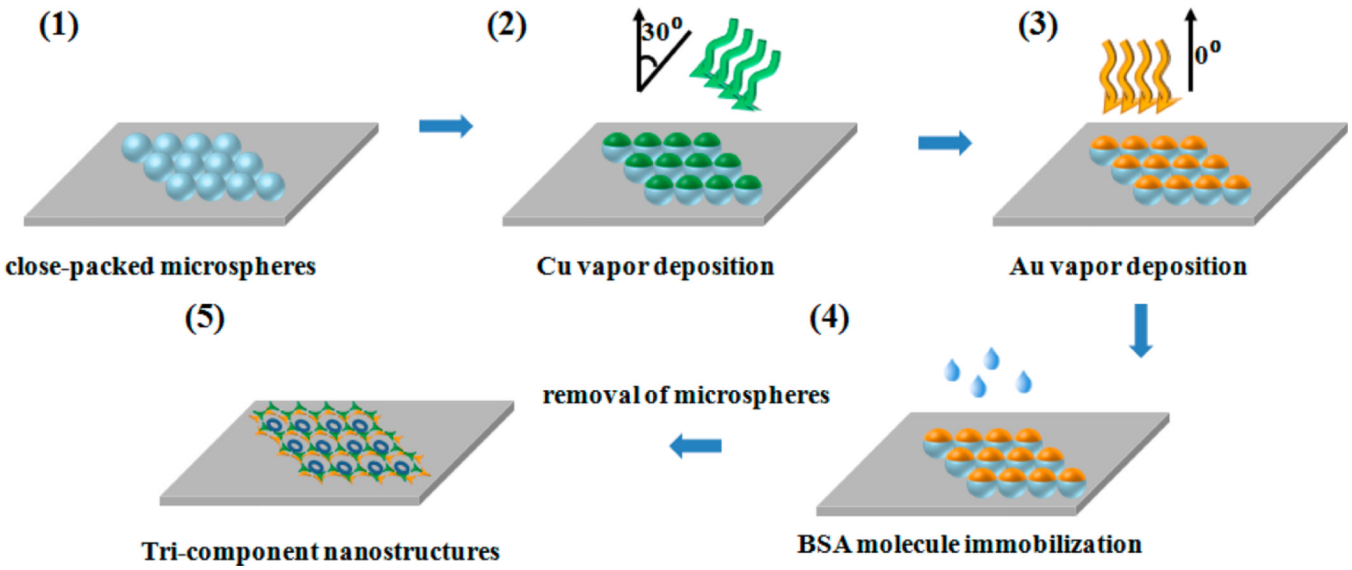

Figure 1.

Key steps for fabricating multicomponent patterns via particle lithography: (1) A monolayer of silica microspheres was formed via drop-dry method on a glass substrate. (2) Cu was deposited via vapor deposition on the glass through the silica particle mask at 30° with respect to the surface normal. (3) Au was deposited via vapor deposition onto the substrate at 0° from the normal. (4) BSA solution was drop cast through the same particle mask and allowed to dry. (5) The silica template was removed via sonication.

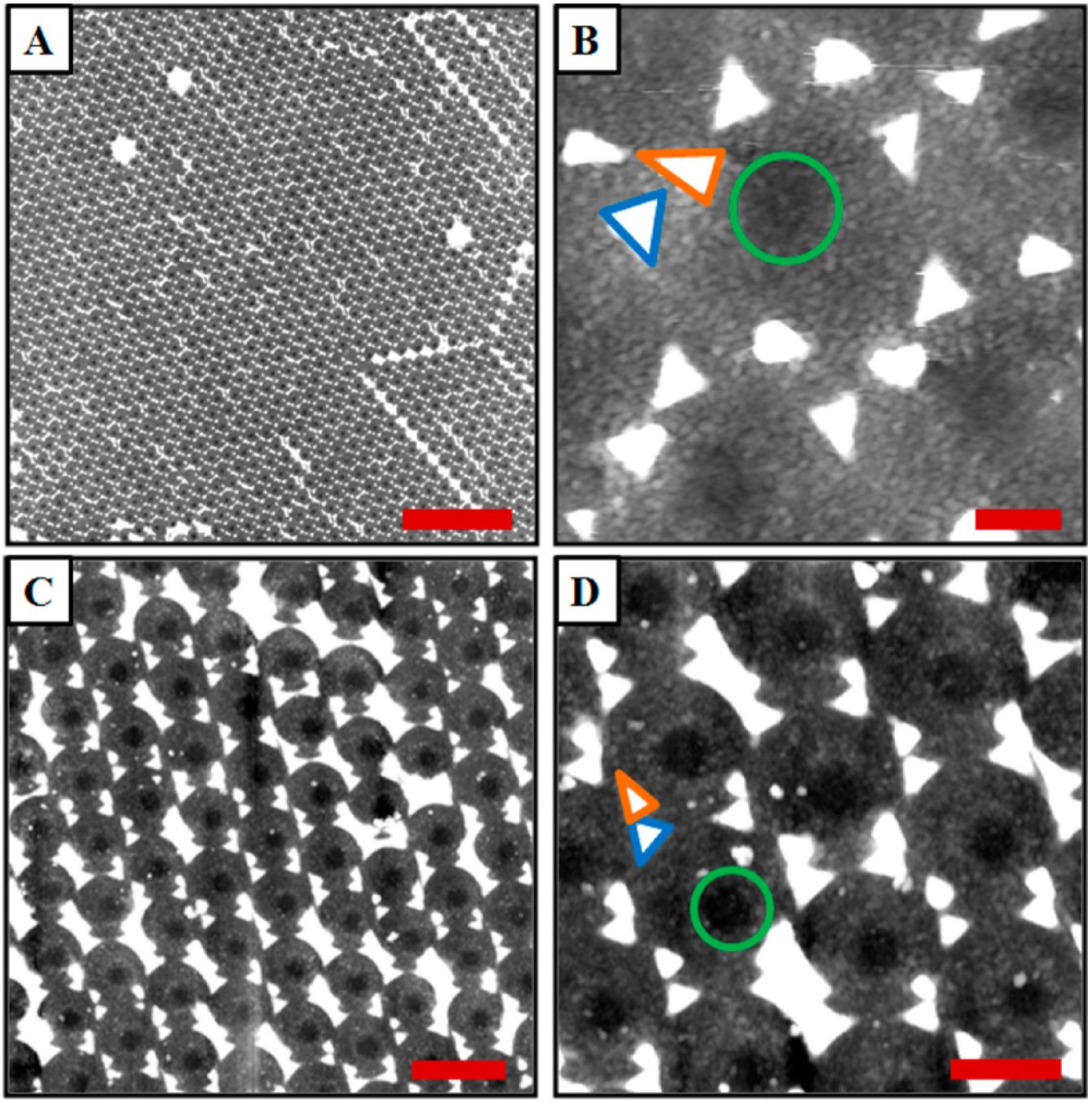

Figure 2.

Patterns composed of Au, Cu, and BSA arrays were fabricated by particle lithography: (A) 50 × 50 μm^2 AFM image of the multicomponent patterns with periodicity of 1.57 μm; (B) zoom-in of (A) revealing the structural details; (C) 5 × 5 μm^2 AFM image of the Au, Cu, and BSA arrays with periodicity of 0.73 μm; (D) zoom-in of (C) revealing the structural details. A Au equilateral triangle, a Cu isosceles triangle, and a BSA circle are highlighted in blue, orange, and green, respectively. The scale bar in (A) is 10 μm; the scale bars in (B) and (D) are 0.5 μm, and the scale bar in (C) is 1 μm.

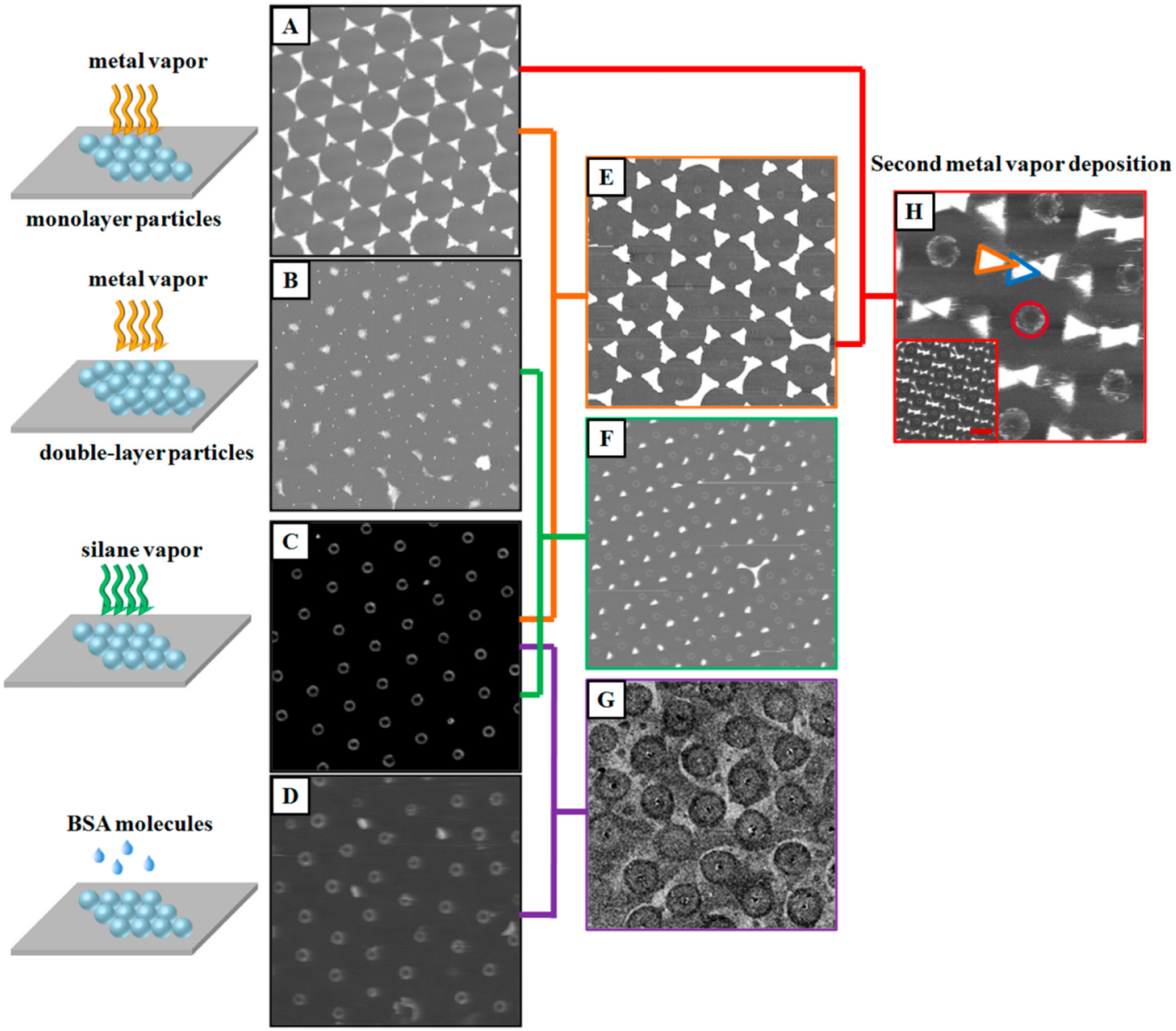

Figure 3.

Particle lithography enables fabrication of nanostructures with different material combinations: (A) 8 × 8 μm^2 AFM image of Au triangular arrays fabricated by vapor deposition of Au through a monolayer particle mask; (B) 8 × 8 μm^2 AFM image of Au dot arrays fabricated by vapor deposition of Au through double-layer of particle mask; (C) 8 × 8 μm^2 AFM image of OTS circular arrays fabricated by deposition of OTS vapor through a monolayer particle mask; (D) 8 × 8 μm^2 AFM image of BSA circular arrays fabricated by drop casting of BSA solution through a monolayer of particle mask; (E) 8 × 8 μm^2 AFM image of Au and PEG-silane arrays; (F) 8 × 8 μm^2 AFM image of Au and OTS arrays; (G) 8 × 8 μm^2 AFM image of OTS and BSA arrays; (H) 4 × 4 μm^2 AFM image of Au, Cu, and PEG-silane arrays. A Au equilateral triangle, a Cu isosceles triangle, and a PEG-silane ring are highlighted in blue, orange, and red, respectively. The inset is zoom-out image of (H); scale bar is 2 μm.